

Multiscale Simulations of Thermal Transport in W-UO₂ CERMET Fuel for Nuclear Thermal Propulsion

Marina Sessim & Michael R. Tonks

To cite this article: Marina Sessim & Michael R. Tonks (2021) Multiscale Simulations of Thermal Transport in W-UO₂ CERMET Fuel for Nuclear Thermal Propulsion, Nuclear Technology, 207:7, 1004-1014, DOI: [10.1080/00295450.2021.1910005](https://doi.org/10.1080/00295450.2021.1910005)

To link to this article: <https://doi.org/10.1080/00295450.2021.1910005>



This material is published by permission of the University of Florida, for the National Aeronautics and Space Administration under Contract No. 80NSSC19K0754 from the Marshall Space Flight Center. The U.S. Government retains for itself, and others acting on its behalf, a paid-up, non-exclusive, and irrevocable worldwide license in said article to reproduce, prepare derivative works, distribute copies to the public, and perform publicly and display publicly, by or on behalf of the Government.



Published online: 06 May 2021.



Submit your article to this journal



Article views: 780



View related articles



View Crossmark data



Multiscale Simulations of Thermal Transport in W-UO₂ CERMET Fuel for Nuclear Thermal Propulsion

Marina Sessim^D and Michael R. Tonks*

University of Florida, Materials Science and Engineering Department, Gainesville, Florida 32611

Received February 22, 2021

Accepted for Publication March 25, 2021

Abstract — Nuclear thermal propulsion (NTP) provides a consistent source of thrust for long space missions. However, fuel development for NTP reactors is a major technological hurdle. Existing modeling and simulation tools developed by the U.S. Nuclear Engineering Advanced Modeling and Simulation (NEAMS) program for power reactors can be leveraged to help accelerate the fuel development. This work is a preliminary demonstration of the application of NEAMS tools to model NTP fuel. Specifically, the fuel performance tool BISON and the mesoscale reactor materials tool MARMOT are used to develop a multiscale model of thermal transport in a W-UO₂ CERMET fuel element for NTP reactors. Three-dimensional simulations in MARMOT are used to estimate the effective thermal conductivity (ETC) of fresh CERMET fuel at temperatures ranging from 1500 K to 3000 K. The ETC values from MARMOT are then used in BISON simulations that predict the steady-state temperature profile throughout a 61-subchannel hexagonal fuel element. The temperature varies by 83 K throughout the fuel element, with the highest temperature occurring near the outer edges of the element. BISON is also used to show that the temperature profile in prototype fuel elements with fewer subchannels does not vary significantly from that in the 61-subchannel element.

Keywords — Multiscale modeling, nuclear thermal propulsion, MOOSE numerical framework.

Note — Some figures may be in color only in the electronic version.

I. INTRODUCTION

The human race has an unceasing curiosity to explore outer space to answer our existential questions. All of our

space exploration up to now has been accomplished using chemical rockets. However, as we consider manned exploration outside of Earth's orbit, other propulsion systems will be needed. One propulsion system being considered for such manned missions is nuclear thermal propulsion (NTP).

The National Aeronautics and Space Administration (NASA) has been interested in NTP since just a few years after the first nuclear reactor produced electricity.¹ Early researchers investigated the application of nuclear fuels to space missions, establishing the baseline of NASA's current NTP project.^{2,3} NTP engines were widely studied starting in the 1960s as part of the Rover/NERVA (Nuclear Engine for Rocket Vehicle Application) Program.^{1–3} The study of NTP engines re-emerged in 2015 when NASA's Nuclear Cryogenic Propulsion Stage project evolved into the NTP project.¹

Nuclear thermal rockets offer a considerable advantage over chemical rockets because they can provide long periods of constant thrust.^{4,5} The nuclear core produces energy by

*E-mail: michael.tonks@ufl.edu

This material is published by permission of the University of Florida, for the National Aeronautics and Space Administration under Contract No. 80NSSC19K0754 from the Marshall Space Flight Center. The U.S. Government retains for itself, and others acting on its behalf, a paid-up, non-exclusive, and irrevocable worldwide license in said article to reproduce, prepare derivative works, distribute copies to the public, and perform publicly and display publicly, by or on behalf of the Government.

This is an Open Access article distributed under the terms of the Creative Commons Attribution-NonCommercial-NoDerivatives License (<http://creativecommons.org/licenses/by-nc-nd/4.0/>), which permits non-commercial re-use, distribution, and reproduction in any medium, provided the original work is properly cited, and is not altered, transformed, or built upon in any way.

fission and is cooled by gaseous hydrogen, which acts as the propellant that provides the necessary thrust. The propellant flows through the subchannels of the fuel elements and absorbs thermal energy, producing an axial temperature difference exceeding 2000 K (Ref. 6). Then, the high-temperature hydrogen gas is exhausted through a nozzle and produces a reaction force that moves the rocket forward. The maneuvers required to reach Mars require multiple restart and short-burn propulsion cycles of the reactor^{7,8} such that the fuel must maintain structural integrity for a combined burn time of under 2 h at very high temperature (2800 to 3000 K) (Refs. 5 and 7). Moreover, a bimodal form of operation has been considered in which the reactor operates at low power and temperature between propulsion cycles to supply a source of electric power [hundreds MW(electric) to 1 MW(electric)] to the spacecraft.^{5,7} The bimodal operation is hard on the fuel due to the combined effects of long-term radiation damage at low temperature and the short high-temperature propulsion cycles. Thus, the fuel conditions in an NTP reactor are quite different from the conditions in a reactor for power generation. For this reason, the design and fabrication of the fuel are a major technological hurdle.¹

One fuel type being considered for NTP reactors is a ceramic-metal composite (CERMET). The CERMET fuel is composed of ceramic fuel particles embedded in a metal matrix. Uranium dioxide (UO₂), uranium carbide (UC), and uranium nitride (UN) are possible uranium-bearing materials with a high enough melting temperature to withstand the conditions during the propulsion cycles. The metal matrix must also have a high enough melting temperature to withstand the propulsion cycles and a higher thermal conductivity than the fuel. Thus, refractory metals such as tungsten (W) or molybdenum (Mo) are the primary candidates. In addition, the neutron absorption cross section of the metal should be as low as possible, as any neutron absorption in the metal matrix will lower the efficiency of the CERMET fuel. Early NTP CERMET fuel designs used highly enriched UO₂ as the fuel particle and W as the metal matrix material.⁷ However, there is now a move to low enrichment, so fuel materials with a higher uranium density than UO₂, such as UN, are being considered.⁹ Molybdenum or a W-Mo alloy is being considered for the matrix, as Mo has a lower neutron absorption cross section than W. Many fuel element designs also include cladding of the fuel element outer surface and the subchannel surfaces. This cladding is often composed of the same material as the metal matrix.

During NTP reactor operation, the CERMET fuel undergoes microstructure evolution that hurts its performance.¹⁰ The most problematic evolution is fissile fuel loss that occurs due to surface vaporization or by vaporization through cracks during

the high-temperature propulsion cycles. Other problematic evolution during the propulsion cycles includes the formation of metal and uranium hydride phases, void formation due to interdiffusion, cracking due to thermal expansion mismatch between the fuel and matrix metal, and even melting. With bimodal operation, low-level amounts of radiation damage and burnup can occur during the low-temperature long-term operation, degrading its thermomechanical properties.⁷ A combined bimodal experiment has not been performed, but CERMET fuels have been tested to high burnups at lower temperatures without significant failure.⁷ Thus, the most significant thermomechanical degradation of the CERMET fuel is expected to occur during the propulsion cycles.

The development and qualification of the NTP fuel will require difficult and expensive testing and could take a significant amount of time and require facilities still under development.⁸ However, the process could be accelerated by using modeling and simulation to assist in the fuel design and reduce the amount of required testing. The U.S. Department of Energy Nuclear Energy Advanced Modeling and Simulation (NEAMS) program has been developing a suite of modeling tools for commercial reactors based on the Multiphysics Object-Oriented Simulation Environment^{11–13} (MOOSE). MOOSE is a numerical framework that significantly simplifies and accelerates the development of advanced modeling tools that solve partial differential equations using the finite element method. The macroscale fuel performance tool BISON predicts the thermomechanical performance of reactor fuel using material models that describe the impact of temperature and burnup on the various properties of the fuel and cladding materials.¹⁴ The mesoscale reactor material tool MARMOT (Ref. 15) predicts the co-evolution of the microstructure and properties of materials during reactor operation. In the multiscale approach used by the NEAMS program,¹⁶ MARMOT is used to investigate the mesoscale material behavior and to inform the development of improved material models for BISON. Neutronics and thermal-hydraulic tools have also been created using the MOOSE framework, and they have been coupled together, along with BISON and MARMOT, for multi-physics reactor core simulations.¹² While developed for power reactors, BISON and MARMOT could be applied to accelerate the development and qualification of NTP fuel.

A complete performance model of a NTP reactor fuel element could be implemented using BISON to predict the temperature and stress fields throughout the element, including the CERMET fuel and subchannel and outer cladding. It would include material models that predict

the thermal and mechanical properties as a function of temperature and the current state of the microstructure. It would use simplified models to represent the neutron flux and thermal and mechanical boundary conditions for stand-alone fuel performance simulations, but it could also be coupled to the MOOSE-based neutronics and thermal-hydraulic tools for multiphysics simulations. The material models for the CERMET fuel and cladding would be developed using information provided by multiphysics mesoscale simulations using MARMOT to determine the effective thermal and mechanical properties and how they are impacted by chemical interaction of the CERMET components with hydrogen, radiation damage, burnup, microcracking due to thermal cycling, and fuel loss. This multiscale approach would result in a powerful fuel performance tool to accelerate the development and optimization of an NTP fuel concept by directly quantifying the impact of the fuel structure on its performance and by determining the probability for failure in beyond-design-basis operation.

The objective of this work is to present a preliminary demonstration of this multiscale modeling and simulation approach using existing capabilities in BISON and MARMOT. We demonstrate this approach by modeling thermal transport through hexagonal CERMET fuel elements using fresh UO₂ fuel particles and a W matrix. We start in Sec. II by analyzing scanning electron microscopy (SEM) images of W-UO₂ CERMET fuels and reconstructing three-dimensional (3-D) microstructures. The effective thermal conductivity (ETC) of the microstructures is calculated using MARMOT for temperatures ranging from 1500 to 3000 K. Then, in Sec. III, the calculated ETC is used in thermal transport simulations using BISON to predict the steady-state temperature profile in hexagonal fuel elements. We conclude in Sec. IV by summarizing our work and discussing how microstructure evolution and property degradation, as well as multiphysics simulations, will be included in the future.

II. ESTIMATION OF THE CERMET ETC AT THE MESOSCALE

In order to model thermal transport through an NTP fuel element, we must know the thermal conductivity of the CERMET. However, there are very little experimental data for the thermal conductivity of W-UO₂ CERMET. In 1968, Grossman² measured the thermal conductivity of W-UO₂ CERMET samples and compared his measurements with predictions from an analytical model by Bruggeman.¹⁷ However, Grossman describes issues with the experimental apparatus that resulted in large errors in

his measured values. In the absence of accurate experimental data, we estimate the fresh CERMET thermal conductivity using MARMOT. We first summarize the method we use to estimate the ETC of W-UO₂ microstructures in Sec. II.A. We then summarize the MARMOT results in Sec. II.B.

II.A. Approach to Estimate CERMET ETC Using MARMOT

The thermal transport in a CERMET nuclear fuel is impacted by a combination of complex processes. At a high level of abstraction, there is the heat generation by fission, the heat conduction through the distinct phases and materials, and heat transfer to the propellant. At the mesoscale, it is important to differentiate the different phases and defects while performing heat conduction analysis. However, resolving the microstructural features is not feasible at the engineering scale. Therefore, we use a hierarchical multiscale approach in which mesoscale simulations are used to calculate the ETC and the homogenized values are then used in the engineering-scale simulations. During NTP reactor operation, the thermal conductivity will decrease with time due to microstructure evolution and defect formation from radiation damage. In this work, we neglect these effects, though they will be included in future work.

We need to estimate the impact of the structure of the UO₂ fuel particles and W matrix on the ETC. The impact of grain boundaries and fission gas bubbles on the thermal conductivity of UO₂ has been estimated by representing the microstructure, assigning local thermal conductivities to the various microstructural features, and then using a steady-state heat conduction solution to quantify the heat transport through the microstructure.^{18–20} We use a similar approach in this work to estimate the ETC of fresh W-UO₂ CERMET fuel. This approach requires an accurate representation of the CERMET microstructure, values for the thermal conductivities of UO₂ and W, and a method for predicting the heat transport. We simplify the estimation by assuming that the interfaces between the W and UO₂ do not have any significant thermal resistance. Consideration of the interfacial thermal resistance will be added in the future.

Figure 1 shows SEM images of example microstructures of W-UO₂ CERMET samples taken from Barnes et al.⁴ The fuel particles are roughly spherical and have a large range in size. However, as these are two-dimensional (2-D) cross sections of a 3-D structure, this size range could result from the actual particle size distribution or because the 2-D sections cut the spherical particles at different positions giving circular cross

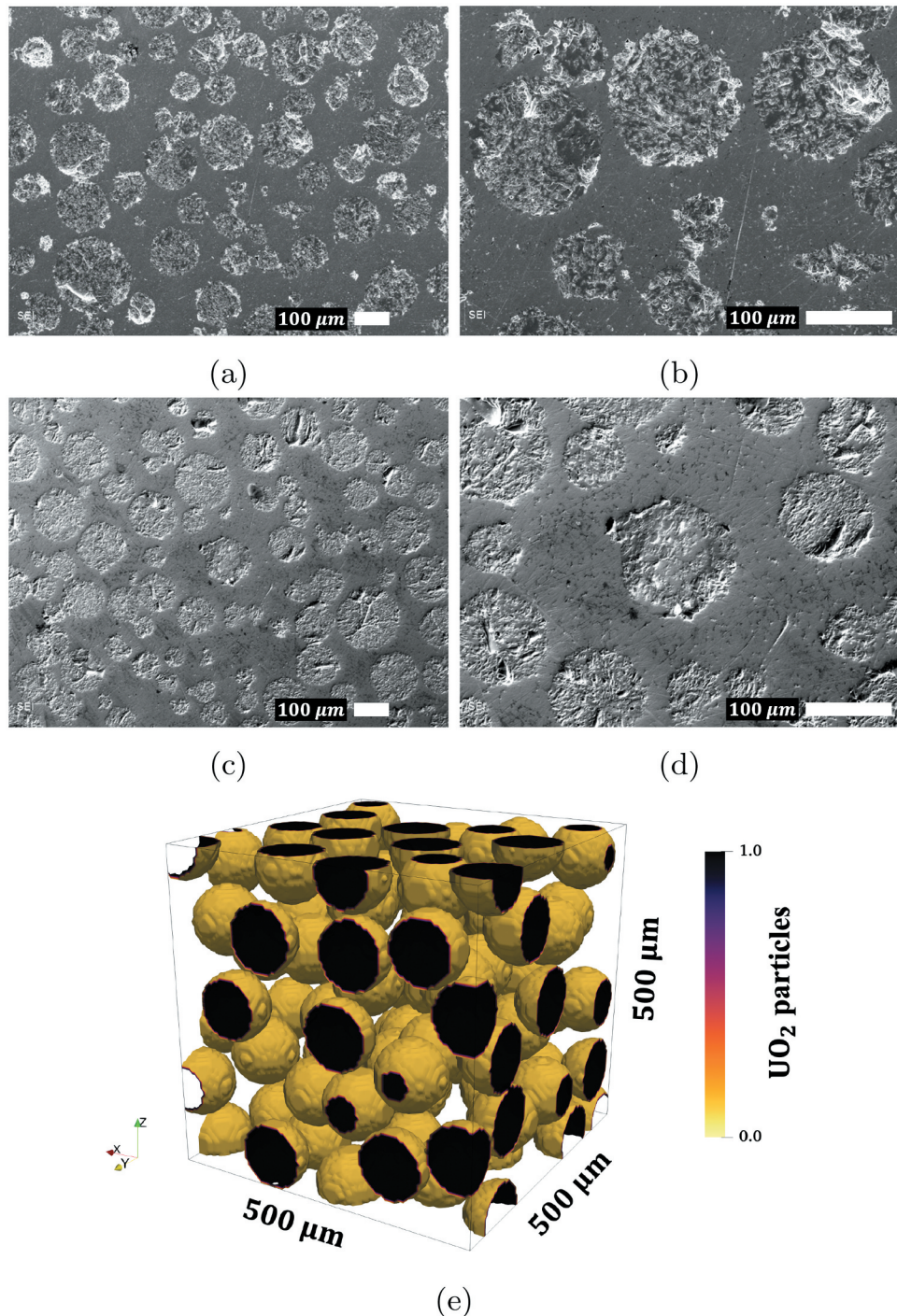


Fig. 1. W-UO₂ CERMET microstructure. (a) through (d) SEM micrographs of W-dUO₂ (depleted UO₂) taken from Barnes et al.⁴; (a) and (b) Samples sintered at 1750°C at 100× and 250× magnification, respectively; (c) and (d) samples sintered at 1800°C at 100× and 250× magnification, respectively. The W matrix is the darker gray region, and the fuel particles are lighter gray. (e) An example of a 3-D CERMET structure generated in MARMOT with 34 vol % UO₂, where only the fuel particles are shown.

sections of various sizes. Barnes et al.⁴ do not provide any information regarding the distribution of fuel particle sizes. Therefore, we assume that the fuel particles have a uniform size. There is also evidence of smaller inclusions in the W matrix. However, for this

work we assume that the matrix is pure W. Finally, it is evident from the SEM images that the fuel particles are not uniformly distributed throughout the matrix. Many of the particles are in contact with other particles.

The SEM images provide only a 2-D picture of the 3-D structure. Therefore, we use the SEM images to illustrate the basic characteristics of the CERMET fuel structure, and we generate fabricated 3-D CERMET microstructures with a similar structure. We generate spherical fuel particles of uniform size within a uniform W matrix. The particles are not uniformly distributed within the matrix and can be in contact with other particles. The UO₂ particles have a spherical shape and a diameter of approximately 100 μm (Ref. 1). Three-dimensional microstructures with various volume fractions of UO₂ are generated using the approach developed by Greenquist et al.²¹ to prepare samples for sintering simulations. The fuel particle positions are determined using a rigid body motion script in which the spheres are randomly placed in a large volume, and then a force is applied to attract the spheres to a specific location. Using this technique, we obtain up to a 54.2 vol % UO₂ microstructure composed of 100-μm-diameter spheres (see Fig. 1e for an example 3-D microstructure).

We obtain the thermal conductivity of UO₂ from Fink,²² who developed an empirical fit to a variety of experimental measurements. The fit considers a large temperature range (using data from 300 to 2900 K) over which different heat transport mechanisms are active. Fink's empirical model for the thermal conductivity of UO₂ (Ref. 22) is

$$k_{\text{UO}_2} = \frac{100}{7.5408 + 17.692t + 3.6142t^2} + \frac{6400}{t^{5/2}} \exp\left(\frac{-16.35}{t}\right), \quad (1)$$

where k_{UO_2} is the thermal conductivity of 95% dense UO₂ in units of W/(m·K) and $t = T(\text{K})/1000$.

For the thermal conductivity of W, we apply the empirical model of Tolias.²³ The author organized the existing thermal conductivity data of tungsten and compared it to the empirical fit proposed by Hust and Lankford.²⁴ The author proposed a modified Hust-Lankford fit that is in excellent agreement with the experimental data and is applicable at high temperatures:

$$k_W = 149.441 - 45.466 \times 10^{-3}T + 13.193 \times 10^{-6}T^2 - 1.484 \times 10^{-9}T^3 + \frac{3.866 \times 10^6}{T^2}, \quad (2)$$

where k_W is the thermal conductivity of tungsten in units of W/(m·K) and T is the temperature in units of kelvin.

We estimate the ETC of the 3-D CERMET microstructures using the finite element method in MARMOT (Ref. 15) to solve the steady-state heat equation. The local thermal conductivity is heterogeneous, with the thermal conductivity from Eq. (1) assigned in the particles and the thermal conductivity from Eq. (2) in the W matrix. We homogenize the local temperature field to estimate the ETC using the asymptotic expansion homogenization (AEH) method that has been implemented in MOOSE (Ref. 25) and is thus available in MARMOT. This method solves the heat equation to calculate the homogenized coefficient that yields the same behavior as the heterogeneous local thermal conductivity in a periodic control volume. The AEH method is more robust than a direct calculation of the ETC because it is not affected by the local temperature field on the boundaries.

II.B. MARMOT CERMET ETC Prediction Results

We first calculate the ETC of the W-UO₂ CERMET at 3000 K for various volume fractions of UO₂ and compare the MARMOT predictions to values from an analytical model. Several analytical models have been developed to predict the ETC of a material with dispersed additive particles. The Rayleigh-Maxwell dilute dispersion equation can be used to calculate the ETC for volume fractions up to 10 to 15 vol %, but this is much smaller than the CERMET volume fraction that is typically around 60%. Bruggeman¹⁷ developed a model that calculates the ETC in a heterogeneous material for any concentration up to the maximum packing fraction of 74.05 vol %:

$$k = k_{\text{UO}_2} + (1 - f_V)(k_W - k_{\text{UO}_2})\left(\frac{k}{k_W}\right)^{1/3}, \quad (3)$$

where k is the ETC and f_V is the volume fraction of UO₂. Volume fractions larger than 74.05% imply that the particles are not uniformly distributed in the matrix. Other models are available for highly anisotropic particles such as ellipsoids; Miller³ proposed an anisotropy correction factor for the Bruggeman model. Webb and Charit²⁶ reviewed the Bruggeman model and the correction proposed by Miller³ for different fuel concepts and found them reasonable for W-UO₂ CERMET fuels. Because of the applicability at higher-volume fractions, we compare the MARMOT predictions to the Bruggeman model.

Figure 2 shows the behavior of the ETC predicted by MARMOT and the Bruggeman model [Eq. (3)] with increasing volume fraction at a temperature of 3000 K.

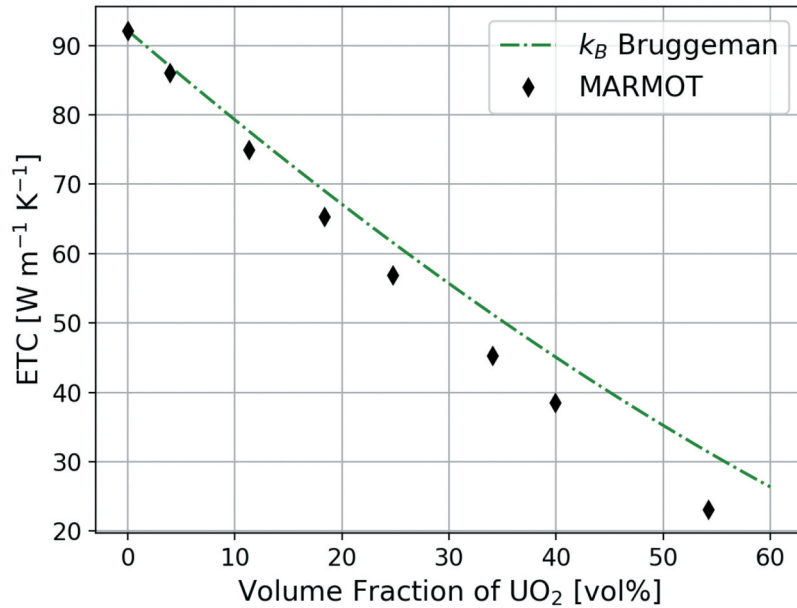


Fig. 2. Estimated ETC values for the W-UO₂ CERMET at 3000 K, where the ETC values are plotted versus volume fraction of UO₂. The values calculated using MARMOT are shown along with the values from the Bruggeman model. The Bruggeman model overpredicts the ETC values compared to the MARMOT results by as much as 40%.

The ETC of the CERMET decreases rapidly with the UO₂ volume fraction since UO₂ has a much lower thermal conductivity than W. For volume fractions greater than 0, the Bruggeman model predicts ETC values that are larger than those predicted by MARMOT. The overprediction of the Bruggeman model increases with the increasing volume fraction of UO₂, overpredicting by almost 40% at 54.2% volume fraction. This is because the Bruggeman model assumes an idealized structure in which the fuel particles are uniformly distributed through the W matrix. However, as shown in Fig. 1, the particles are not uniformly distributed and are often in contact with other particles. The 3-D microstructures used in MARMOT are generated to have similar characteristics to actual CERMET microstructures, and therefore, MARMOT more accurately predicts the CERMET ETC. Moreover, MARMOT also has the capability to model the evolution of the microstructure and the resultant degradation of the thermal and mechanical properties during reactor operation, which will be used in future work.

For use in BISON, we need to know the ETC of the CERMET fuel for volume fractions near 60% and for typical operating temperatures of NTP reactors. Therefore, we calculate the ETC using MARMOT for the 3-D microstructure with 54.2 vol % UO₂ at temperatures ranging from 1500 to 3000 K. In order to obtain a continuous profile of the calculated ETC with temperature, we fit the data obtained using MARMOT to a simple expression:

$$k = 25.594 - \frac{1.5331 \times 10^4}{T} + \frac{2.3675 \times 10^7}{T^2} , \quad (4)$$

where k is the ETC of the reconstructed microstructure in units of W/(m·K) and T is the temperature in units of kelvin. Figure 3 shows the MARMOT-calculated values, the fitted ETC curve [Eq. (4)], and the empirical fits for the thermal conductivity of UO₂ [Eq. (1)] and W [Eq. (2)]. The W thermal conductivity is more than an order of magnitude larger than the UO₂ thermal conductivity and decreases with temperature from 1500 to 3000 K. The UO₂ thermal conductivity decreases with temperature from 1500 K to around 2000 K and then increases with temperature. However, since the CERMET ETC is dominated by W, the ETC values predicted by MARMOT decrease with temperature through the full temperature range, though they only change by about 3 W/(m·K) from 1500 to 3000 K.

III. THERMAL PERFORMANCE AT THE ENGINEERING SCALE

The ETC values calculated using MARMOT are now used in BISON fuel performance simulations as part of our multiscale approach. Hexagonal fuel elements are strong candidates for NTP. The flow of propellant through the subchannels cools the reactor core, and the

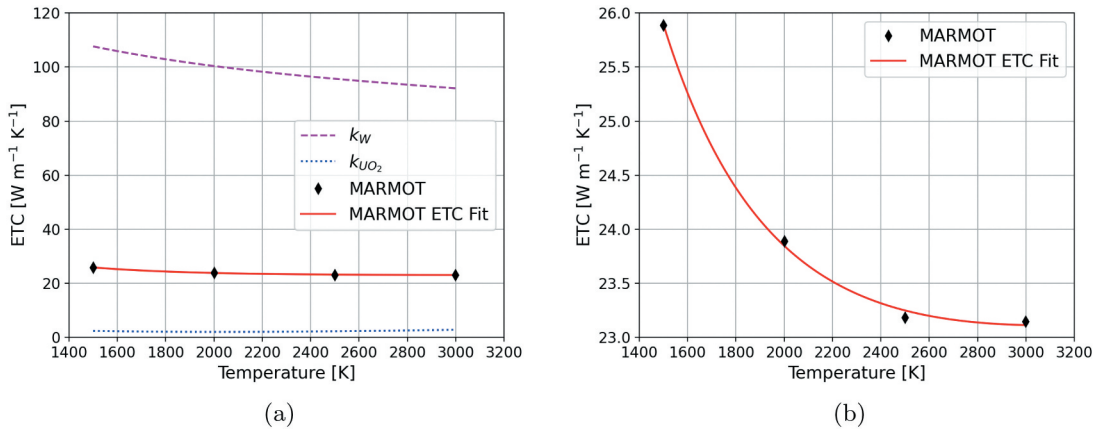


Fig. 3. Calculated ETC values and the fitted curve for a W-UO₂ CERMET with 54.2 vol % UO₂ for temperatures ranging from 1500 to 3000 K. (a) Comparison between the ETC values calculated using MARMOT and the individual thermal conductivities of W [Eq. (2)] and UO₂ [Eq. (1)]. (b) Plot showing only the ETC values calculated by MARMOT and the fitted curve.

heated gas is exhausted, creating thrust to propel the rocket. The 61-subchannel fuel element is a potential candidate to become the NTP fuel,²⁷ though concepts with more subchannels are also being considered. Fuel elements with more, closely spaced subchannels have a better surface cooling area-to-volume of fuel ratio and thus have more effective heat transfer to the propellant.²⁸ The manufacturing process becomes increasingly difficult as the number of subchannels increases, and often, elements with fewer subchannels are used as prototypes for the final fuel concept. In this work, we predict the steady-state temperature profile

throughout a 61-subchannel element. We also predict the steady-state temperature profile throughout 7- and 19-subchannel elements to investigate possible differences in the temperature profiles of such prototypes compared to that in the 61-subchannel candidate element.

Figure 4 shows the geometry of the 61-subchannel hexagonal fuel element, depicting the dimensions used in this work. The bulk of the element is filled with W-UO₂ CERMET, with a microstructure similar to those shown in Fig. 1. There is a layer of pure W cladding around the subchannels to protect the fuel from the propellant, to avoid fuel loss to the propellant. Furthermore, there is

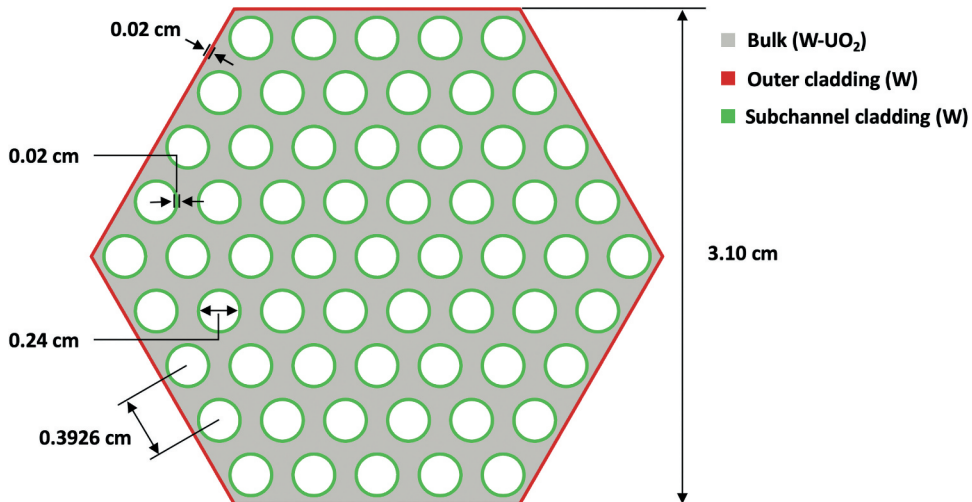


Fig. 4. Top view of the 61-subchannel fuel concept with depicted dimensions. The bulk (gray) consists of W-UO₂ CERMET; the outer cladding (red) and subchannel cladding (green) are considered to be W. The 7- and 19-subchannel concepts differ only in their heights, assuming values of 1.17 and 1.81 cm, respectively. The in-plane thickness for all concepts is assumed to be 1 cm.

a layer of W cladding on the outer side of the hexagonal structure. We also analyze hexagonal fuel concepts with 7 and 19 subchannels. The subchannel diameter and the distance between subchannels is the same in each concept, such that they differ only in their heights, where the 7-subchannel element has a height of 1.17 cm, the 19-subchannel element has a height of 1.81 cm, and the 61-subchannel element has a height of 3.1 cm. We consider only a small section of the fuel element in the axial direction, with an axial thickness of 1 cm. Actual fuel elements would be much thicker, and more realistic thicknesses will be modeled in future work.

We use the BISON fuel performance tool¹⁴ to predict the steady-state temperature profile throughout the 7-, 19-, and 61-subchannel hexagonal fuel elements. The temperature is calculated by solving the steady-state heat conduction equation:

$$\cdot k(\vec{r}, T) \cdot T(\vec{r}, T) + \dot{q}(\vec{r}) = 0 , \quad (5)$$

where

$k(\vec{r}, T)$ = thermal conductivity at a given position \vec{r} and temperature T

\dot{q} = heat generation due to fission that is only nonzero in the bulk.

For the thermal conductivity of the bulk, we apply the ETC fit from Eq. (4), which assumes a CERMET with 54.2 vol % UO₂. For the thermal conductivity of the W cladding, we use Eq. (2). For the heat generation due to fission, we use $\dot{q} = 5 \times 10^3$ W/cm³ in the bulk of the fuel element, based on the work of Stewart and Schnitzler,²⁹ and $\dot{q} = 0$ in the cladding. More realistic power generation that varies throughout the fuel elements will be obtained in the future by coupling to neutron transport simulations.

We need boundary conditions for the outer boundaries of the hexagonal fuel element and for the subchannel boundaries. For the outer boundaries, we assume zero flux boundary conditions. This is a symmetry boundary condition that mimics the behavior of an infinite network of interlocking hexagonal elements. The coolant flowing through the subchannels cools the fuel element via convection. We approximate this cooling with a simple Dirichlet boundary condition using a fixed temperature of 1500 K at the subchannel boundaries, with no axial variation through the 1-cm thickness of our fuel elements. As mentioned previously, actual fuel elements could experience axial temperature changes of as much as 2000 K (Ref. 6). Realistic axial temperature profiles

will be obtained in the future by coupling to thermal-hydraulic simulations.

Figure 5a shows the temperature throughout the 61-subchannel concept. The temperature profile is uniform in the axial direction, due to our assumptions that the heat generation and subchannel boundary conditions are uniform. The temperature is heterogeneous across the fuel element, varying by 83 K from the hottest to the coolest regions. The coolest regions of the fuel element are the subchannel surfaces, due to our assumed boundary condition. The hottest regions of the fuel element occur near the outer boundaries of the hexagonal fuel element, at the regions in the element that are farthest from the subchannels.

As stated above, prototype fuel elements with fewer subchannels are often used to simplify fabrication. However, it is important to know how the temperature profile in these prototype fuel elements differs from the temperature profile in the actual fuel element concept. Figure 5b shows the steady-state temperature profiles predicted by the BISON simulations for the 7-, 19-, and 61-subchannel fuel elements. It is clear that the temperature profiles are similar in the three fuel elements. Table I shows the average and maximum temperatures in the three fuel elements (the minimum temperature is 1500 K in all three cases, due to the assumed subchannel boundary condition). It also shows the subchannel surface area-to-fuel volume (A/V) ratio. The average and maximum temperatures in the three fuel elements vary by only 1 K. The A/V ratio decreases as the number of subchannels increases, though it only varies by 6%. The average and maximum temperatures decrease with the increasing A/V ratio. These results demonstrate that the fuel elements with fewer subchannels do have similar thermal behavior to the fuel 61-subchannel fuel element concept.

TABLE I
Comparison Between the Temperature Profile in the 7-, 19-, and 61-Subchannel Fuel Elements

Subchannels	A/V Ratio (cm ⁻¹)	Average T (K)	Maximum T (K)
7	11.22	1544.0	1581.7
19	10.74	1545.0	1582.2
61	10.55	1544.9	1582.7

*The columns show the ratio of the subchannel surface area to the fuel volume (A/V ratio) and the average and maximum temperatures in the bulk region of the hexagonal fuel.

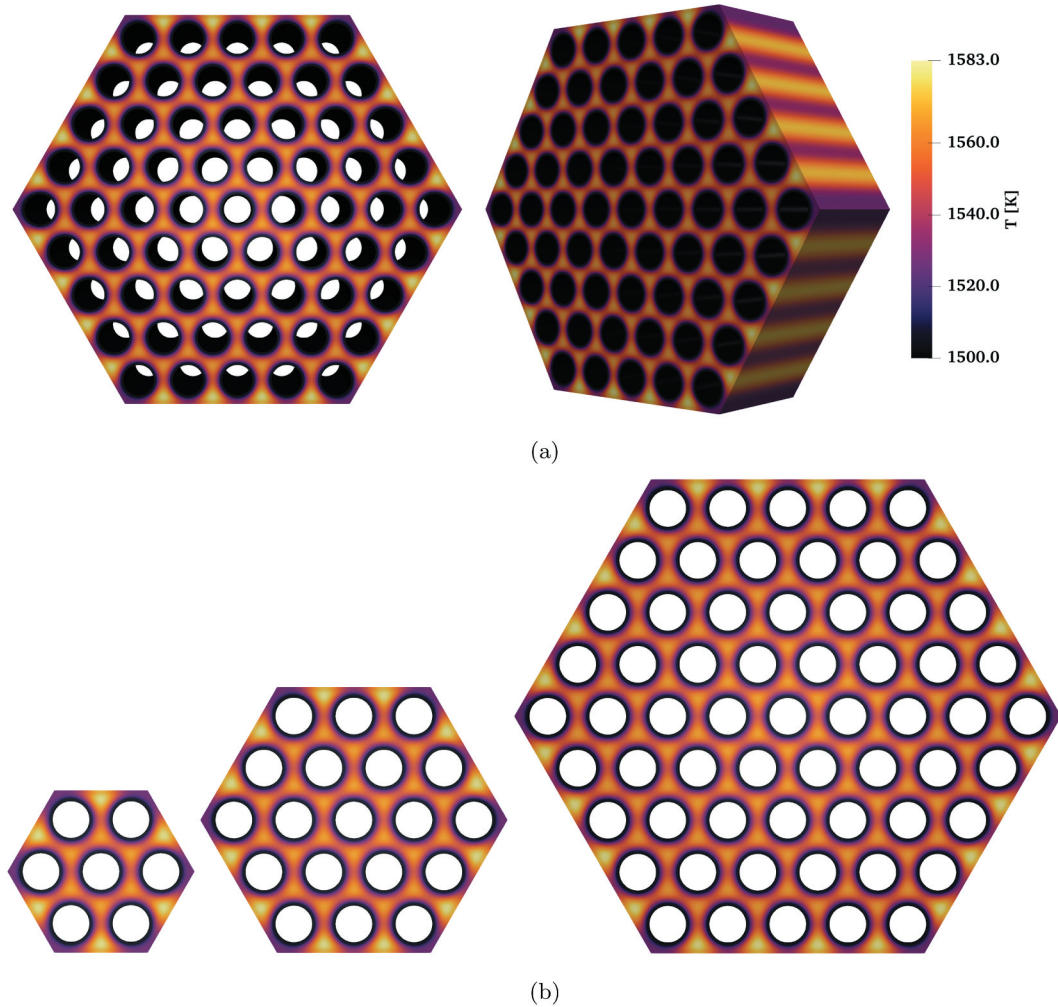


Fig. 5. Temperature profile of the hexagonal NTP fuel elements predicted by BISON. (a) Detailed view of the temperature profile in the 61-subchannel element. (b) Temperature profile on the front face of the fuel elements, with the 7-subchannel element on the left, the 19-subchannel element in the center, and the 61-subchannel element on the right. The elements are shaded by temperature, and the images in (a) and (b) use the same temperature scale.

IV. CONCLUSION

The development of CERMET fuels for NTP reactors will be expensive and time-consuming. However, modeling and simulation could help reduce cost and time. In this work, we have demonstrated how the capabilities of the MARMOT and BISON tools, developed by the NEAMS program for power reactors, can be leveraged to create a multiscale modeling and simulation approach to assist the development of NTP CERMET fuel. In our preliminary demonstration, we modeled the thermal transport within fresh W-UO₂ CERMET fuel elements.

The thermal conductivity of a W-UO₂ CERMET depends on the temperature, volume fraction of UO₂, and microstructure of the CERMET. Accurate values for the CERMET thermal conductivity are not available from

experiments, so we used MARMOT to estimate the ETC of 3-D CERMET microstructures. We used SEM images to identify the basic characteristics of the microstructure. We then generated 3-D structures with similar characteristics. The ETC calculated by MARMOT was lower than that predicted by the Bruggeman analytical model, likely due to the assumption in the Bruggeman model that the fuel particles are uniformly distributed in the matrix. An equation was fit to the MARMOT-calculated ETC values, and it was used in BISON as the thermal conductivity of the fuel. The steady-state temperature profile in a 61-subchannel fuel element was determined, with the temperature varying by 83 K across the element. The hottest regions were near the outer boundaries of the hexagon element. BISON was also used to model the steady-state temperature profile in prototype fuel elements with fewer

numbers of coolant subchannels. The temperature profiles were very similar, with the maximum temperatures varying by only 1 K.

This work used a simple model of steady-state heat transport to demonstrate how the existing capabilities in MARMOT and BISON can be applied to NTP reactor fuel. We will continue this multiscale modeling and simulation effort to help accelerate NTP fuel development. MARMOT will be used to investigate microstructure evolution that takes place within the fuel during both the high-temperature propulsion cycles and long-term low-temperature operation for power generation. Specifically, we will investigate fuel loss by developing models of the chemical reactions with hydrogen, including the formation of hydride phases, as well as microcracking due to thermal expansion and phase transformation. We will also calculate the impact of these changes, as well as radiation damage, on the thermal conductivity and other thermal and mechanical properties. The information from the MARMOT simulations will then be used to develop material models that will be implemented in BISON.

The improved material models will be a critical step toward developing an accurate fuel performance capability for NTP fuel in BISON. However, improvements are also needed in the representation of the heat generation due to fission and the temperature boundary conditions in the coolant subchannels. We will take advantage of the easy coupling of multiphysics applications using MOOSE (Ref. 12) to couple BISON to a neutronics solver to estimate the fission heat source and to a thermal-hydraulic model to simulate the coolant flow and the resultant subchannel cooling rates and axial temperature change. This robust multiscale multiphysics approach will aid the investigation of prospective NTP fuels by analyzing their performance during realistic operating conditions.

Acknowledgments

The authors would like to acknowledge Marvin Barnes and Robert Hickman from the NASA Marshall Space Flight Center for their scientific guidance and valuable discussions. This research was supported by NASA through a subcontract from the NASA Marshall Space Flight Center to The Pennsylvania State University.

ORCID

Marina Sessim  <http://orcid.org/0000-0001-9805-2279>

References

- R. R. HICKMAN et al., "Fabrication and Testing of CERMET Fuel Materials for Nuclear Thermal Propulsion," *Proc. 48th AIAA/ASME/SAE/ASEE Joint Propulsion Conf.*, Atlanta, Georgia, July 30–August 1, 2012, American Institute of Aeronautics and Astronautics (2012); <http://ntrs.nasa.gov/archive/nasa/casi.ntrs.nasa.gov/20120015797.pdf> (current as of Feb. 22, 2021).
- L. N. GROSSMAN, "Thermal Conductivity of Coated Particle UO₂-Tungsten Cermets," NASA-CR-1154, National Aeronautics and Space Administration (1968).
- J. V. MILLER, "Estimating Thermal Conductivity of CERMET Fuel Materials for Nuclear Reactor Application," NASA-TN-D-3898, National Aeronautics and Space Administration (1967).
- M. W. BARNES et al., "Nuclear Rocket Ceramic Metal Fuel Fabrication Using Tungsten Powder Coating and Spark Plasma Sintering," NASA/TP-2017-218236, National Aeronautics and Space Administration (2017).
- S. K. BOROWSKI, D. R. McCURDY, and T. W. PACKARD, "Nuclear Thermal Propulsion (NTP): A Proven Growth Technology for Human NEO/Mars Exploration Missions," NASA/TM-2014-218104, National Aeronautics Space Administration (2014); <https://doi.org/10.1109/AERO.2012.6187301>.
- J. ZHANG et al., "Design Research for the Porous Hexagonal Prism Shaped Fuel Element Adopted in Nuclear Thermal Propulsion Reactor Based on Neutronics and Thermal-Hydraulics Coupled Method," *Ann. Nucl. Energy*, **150**, 107847 (2021); <https://doi.org/10.1016/j.anucene.2020.107847>.
- S. K. BHATTACHARYYA, "An Assessment of Fuels for Nuclear Thermal Propulsion," Argonne National Laboratory (2002); <https://doi.org/10.2172/822135>.
- R. H. HOWARD and A. E. RUGGLES, "Design and Out-of-Pile Testing of a Novel Irradiation Experiment Vehicle to Support Qualification of Nuclear Thermal Propulsion Components," *Nucl. Eng. Des.*, **361**, 110516 (2020); <https://doi.org/10.1016/j.nucengdes.2020.110516>.
- M. KRECICKI and D. KOTLYAR, "Low Enriched Nuclear Thermal Propulsion Neutronic, Thermal Hydraulic, and System Design Space Analysis," *Nucl. Eng. Des.*, **363**, 110605 (2020); <https://doi.org/10.1016/j.nucengdes.2020.110605>.
- C. HAERTLING and R. J. HANRAHAN, "Literature Review of Thermal and Radiation Performance Parameters for High-Temperature, Uranium Dioxide Fueled Cermet Materials," *J. Nucl. Mater.*, **366**, 3, 317 (2007); <https://doi.org/10.1016/j.jnucmat.2007.03.024>.
- D. GASTON et al., "MOOSE: A Parallel Computational Framework for Coupled Systems of Nonlinear Equations,"

- Nucl. Eng. Des.*, **239**, 10, 1768 (2009); <https://doi.org/10.1016/j.nucengdes.2009.05.021>.
12. D. R. GASTON et al., “Physics-Based Multiscale Coupling for Full Core Nuclear Reactor Simulation,” *Ann. Nucl. Energy*, **84**, 45 (2015); <https://doi.org/10.1016/j.anucene.2014.09.060>.
 13. C. J. PERMANN et al., “MOOSE: Enabling Massively Parallel Multiphysics Simulation,” *SoftwareX*, **11**, 100430 (2020); <https://doi.org/10.1016/j.softx.2020.100430>.
 14. R. L. WILLIAMSON et al., “Multidimensional Multiphysics Simulation of Nuclear Fuel Behavior,” *J. Nucl. Mater.*, **423**, 1–3, 149 (2012); <https://doi.org/10.1016/j.jnucmat.2012.01.012>.
 15. M. R. TONKS et al., “An Object-Oriented Finite Element Framework for Multiphysics Phase Field Simulations,” *Comput. Mater. Sci.*, **51**, 1, 20 (2012); <https://doi.org/10.1016/j.commatsci.2011.07.028>.
 16. M. R. TONKS et al., “Mechanistic Materials Modeling for Nuclear Fuel Performance,” *Ann. Nucl. Energy*, **105**, 11 (2017); <https://doi.org/10.1016/j.anucene.2017.03.005>.
 17. D. A. G. BRUGGEMAN, “Berechnung verschiedener physikalischer Konstanten von heterogenen Substanzen I. Dielektrizitätskonstanten und Leitfähigkeiten der Mischkörper aus isotropen Substanzen,” *Ann. Phys.*, **421**, 2, 160 (1937); <https://doi.org/10.1002/andp.19374210205>.
 18. P. C. MILLETT and M. TONKS, “Meso-Scale Modeling of the Influence of Intergranular Gas Bubbles on Effective Thermal Conductivity,” *J. Nucl. Mater.*, **412**, 3, 281 (2011); <https://doi.org/10.1016/j.jnucmat.2011.02.040>.
 19. P. C. MILLETT et al., “Three Dimensional Calculations of the Effective Kapitza Resistance of UO₂ Grain Boundaries Containing Intergranular Bubbles,” *J. Nucl. Mater.*, **439**, 1–3, 117 (2013); <https://doi.org/10.1016/j.jnucmat.2013.02.039>.
 20. M. R. TONKS et al., “Development of a Multiscale Thermal Conductivity Model for Fission Gas in UO₂,” *J. Nucl. Mater.*, **469**, 89 (2016); <https://doi.org/10.1016/j.jnucmat.2015.11.042>.
 21. I. GREENQUIST et al., “Development of a Microstructural Grand Potential-Based Sintering Model,” *Comput. Mater. Sci.*, **172**, 109288 (2020); <https://doi.org/10.1016/j.commatsci.2019.109288>.
 22. J. FINK, “Thermophysical Properties of Uranium Dioxide,” *J. Nucl. Mater.*, **279**, 1, 1 (2000); [https://doi.org/10.1016/S0022-3115\(99\)00273-1](https://doi.org/10.1016/S0022-3115(99)00273-1).
 23. P. TOLIAS, “Analytical Expressions for Thermophysical Properties of Solid and Liquid Tungsten Relevant for Fusion Applications,” *Nucl. Mater. Energy*, **13**, 42 (2017); <https://doi.org/10.1016/j.nme.2017.08.002>.
 24. J. G. HUST and A. B. LANKFORD, “Thermal Conductivity of Aluminum, Copper, Iron, and Tungsten for Temperatures from 1 K to the Melting Point,” NBSIR 84-3007, National Bureau of Standards (1984).
 25. J. HALES et al., “Asymptotic Expansion Homogenization for Multiscale Nuclear Fuel Analysis,” *Comput. Mater. Sci.*, **99**, 290 (2015); <https://doi.org/10.1016/j.commatsci.2014.12.039>.
 26. J. A. WEBB and I. CHARIT, “Analytical Determination of Thermal Conductivity of W-UO₂ and W-UN CERMET Nuclear Fuels,” *J. Nucl. Mater.*, **427**, 1–3, 87 (2012); <https://doi.org/10.1016/j.jnucmat.2012.04.020>.
 27. S. K. BOROWSKI et al., “Affordable Development and Demonstration of a Small NTR Engine and Stage: A Preliminary NASA, DOE and Industry Assessment,” *Proc. 51st AIAA/ASME/SAE/ASEE Joint Propulsion Conf.*, Orlando, Florida, July 27–29, 2015, American Institute of Aeronautics and Astronautics (2015); <https://doi.org/10.2514/6.2015-3774>.
 28. J. WEBB, B. GROSS, and W. TAITANO, “Conceptual Design of a CERMET NTR Fission Core Using Multiphysics Modeling Techniques,” *Proc. 47th AIAA/ASME/SAE/ASEE Joint Propulsion Conf.*, San Diego, California, July 31–August 2, 2011, American Institute of Aeronautics and Astronautics (2011); <https://doi.org/10.2514/6.2011-5947>.
 29. M. STEWART and B. SCHNITZLER, “Thermal, Fluid, and Structural Analysis of a Cermet Fuel Element,” *Proc. 48th AIAA/ASME/SAE/ASEE Joint Propulsion Conf.*, Atlanta, Georgia, July 30–August 1, 2012, American Institute of Aeronautics and Astronautics (2012); <https://doi.org/10.2514/6.2012-3959>.